



Modelling of Ocean Circulation in the Newfoundland Basin

by

© **Kyle Pike**

A thesis submitted to the Department of Physics and
Physical Oceanography in partial fulfillment of the
requirements for the degree of Bachelor of Science
(Honours).

Department of Physics and Physical Oceanography
Memorial University

May 2025

St. John's, Newfoundland and Labrador, Canada

Abstract

The average temperature of the Earth's surface has increased significantly since pre-industrial levels and continues to rise. This global warming is caused by the increased level of greenhouse gases in the atmosphere, particularly carbon dioxide (CO_2). To reduce the rate of temperature increase, it is necessary to decrease the amount of CO_2 in the atmosphere. One way to achieve this is by allowing oceans to absorb more CO_2 through a process known as ocean alkalinity enhancement (OAE), which occurs when alkaline particles are added to the ocean surface. The observational tracking of particle trajectories through the ocean presents significant challenges; therefore, ocean models are primary tools for predicting particle trajectories. This research focuses on ocean modelling around the Newfoundland Basin. The Regional Ocean Modelling System (ROMS) has been implemented for this region. ROMS is a hydrostatic, free-surface ocean model which uses a terrain-following vertical coordinate. The continuous model equations of ROMS, along with their numerical implementations, are described. The model initialization, as well as the definition of surface forcing and boundary conditions, are presented. The method of particle tracking in ROMS is described. Preliminary results from model simulations of ocean characteristics, including ocean temperature, salinity, and sea surface height, for July 2020 are outlined. Particle trajectories after a month of circulation within the Newfoundland Basin are shown. Future work, including extended model duration and different particle distribution methods, is then discussed in the context of applications to OAE.

Acknowledgements

I would like to thank my supervisors, Dr. Entcho Demirov and Dr. Kris Poduska for all of their help with working on this project and with editing of this thesis.

I would also like to thank the Digital Research Alliance of Canada for allowing me to use their computational resources.

Table of contents

Title page	i
Abstract	ii
Acknowledgements	iii
Table of contents	iv
List of figures	vi
List of abbreviations	viii
1 Introduction	1
1.1 Climate change	1
1.2 Motivation	3
2 Regional Ocean Modeling System (ROMS) features	5
2.1 Model Equations	5
2.2 Vertical coordinate system	7
2.3 Boundary conditions	9
2.4 Grid structure	11
3 Model Implementation	14

3.1	Grid building	14
3.2	Atmospheric forcing	14
3.3	Initial conditions	17
3.4	Particle tracers	21
4	Results	22
4.1	The sea surface height	22
4.2	The sea surface temperature	24
4.3	The sea surface salinity	26
4.4	Particle trajectories	28
5	Conclusion	30
	Bibliography	32
A	Alternate formulations of equations of ocean dynamics	34
A.1	Using sigma coordinates	34
A.2	Using curvilinear coordinates	36
B	Other stretching functions for terrain following vertical coordinates in ROMS	38
C	Vertical mixing parameters	40
D	Atmospheric forcing and initial conditions creation	43
D.1	Atmospheric forcing creation	43
D.2	Initial conditions creation	44

List of figures

1.1	Model results for atmospheric CO ₂ , temperature anomaly, net land carbon flux and net ocean carbon flux from various models using Coupled Model Intercomparison Project Phase 6 (CMIP6) and observational data. The x-axis is years in all the plots. The black line represents the observational data, the red line is the mean of all the models used, and every other line is an individual model that can be determined using the colour coded legend in all plots. Figure 3.31 in[11].	2
2.1	Terrain-following vertical coordinate. From ROMS wiki, February 29 2008, https://www.myroms.org/wiki/File:vieste-dubrovnik.png , obtained April 27, 2025.	8
2.2	Arakaw C grid It shows where each value is calculated on each grid point. The u velocity component is calculated at the boundaries in the x direction, the v velocity component is calculated at the boundaries in the y direction, and all other values, denoted by ρ are calculated at the center of the cell. From ROMS wiki, May 6 2016, https://www.myroms.org/wiki/File:nesting_staggered_grid_rho_cells.png , obtained on April 23, 2025.	12
2.3	Staggered vertical grid used in ROMS. From ROMS wiki, March 7 2008, https://www.myroms.org/wiki/File:vertical_grid.png , obtained April 23, 2025.	13
3.1	Bathymetry in the Newfoundland Basin and its surrounding region. The colour bar depicts ocean depth in units of meters.	15

3.2	Sea surface temperature on July 1, 2020 at 12:00 p.m. Data is obtained from the dataset ERA5 hourly data on single levels from 1940 to present. The colour bar has units of °C.	16
3.3	Initial condition for the SSH at 12:00 p.m. on July 1, 2020. The colour bar units are meters.	18
3.4	Initial condition for temperature at the ocean surface at 12:00 p.m on July 1, 2020. The colour bar units are °C.	19
3.5	Initial condition for salinity at the ocean surface at 12:00 p.m on July 1, 2020. The colour bar represents the grams of salt per kilogram of water (g/kg).	20
4.1	SSH at 12:00 p.m. on July 31, 2020. The colour bar units are meters. .	23
4.2	Sea surface temperature at 12:00 p.m. on July 31, 2020. The colour bar units are °C.	25
4.3	Sea surface salinity at 12:00 p.m. on July 31, 2020. The colour bar represents how many grams of salt there are per kilogram of water. . .	27
4.4	Trajectory of 100 particles during the month July 2020. The red dots represent the initial positions at 12:00 p.m. on July 1, 2020, the black dots denote the final positions projected onto the surface at 12:00 p.m. on July 31, 2020, and the white lines indicate the trajectories they followed throughout the month. The top figure shows the trajectories about the entire model domain. The bottom figure is zoomed in to show the individual trajectories. In both figures the x-axis is latitude and the y-axis is longitude. The top figure has a latitude range of -60 to -40 and a longitude range of 42 to 56. The bottom figures has a latitude range of -52.6 to -51 and a longitude range from 50 to 51.5. In both figures the colour bar is the SSH and ranges from 0 to -1.	29

List of abbreviations

GHG	Greenhouse Gas
CO ₂	Carbon Dioxide
CDR	Carbon Dioxide Demoval
MCDR	Marine Carbon Dioxide Removal
OAE	Ocean Alkalinity Enhancement
ROMS	Regional Ocean Modeling System
MMRV	Monitoring, Measuring, Reporting, and Verification
GEBCO	General Bathymetric Chart of the Oceans
ECMWF	European Centre for Medium-Range Weather Forecasts
SSH	Sea Surface Height
SST	Sea Surface Temperature
SSS	Sea Surface Salinity

Chapter 1

Introduction

1.1 Climate change

The average surface temperature of the Earth has been rapidly increasing since the industrial revolution. The reason for this is due to the increasing amount of greenhouse gas (GHG) in the atmosphere, which affects the average global temperature of the Earth. One of the most common GHGs that is causing this phenomenon is carbon dioxide (CO₂)[4]. Human activities have increased the amount of atmospheric CO₂ by over 50% when compared to levels before the industrial revolution[10]. Due to the increase in human produced CO₂ the average temperature of the atmosphere has been steadily increasing and is now rapidly approaching 1.5°C above preindustrial levels[6]. 1.1 shows the impact that an increase in CO₂ has on global temperature anomaly, as well as the net land and ocean carbon fluxes.

The Paris Agreement is an international climate initiative to keep the average global temperature below a 2.0°C increase compared to preindustrial levels[14]. In order to reach this goal, the amount of atmospheric CO₂ must be reduced. For this to happen, the production of CO₂ must be reduced and the current levels have to decrease. Neither carbon dioxide removal (CDR) methods or reduced emissions are enough to reach a net negative CO₂ emission level, so both will have to be used in order to reach this goal[4]. To lower current levels, CDR methods must be implemented. A reduction in the global CO₂ levels will lead to a lower global temperature increase that will eventually reach closer to preindustrial levels.

A specific category of CDR methods are those that use the oceans, known as

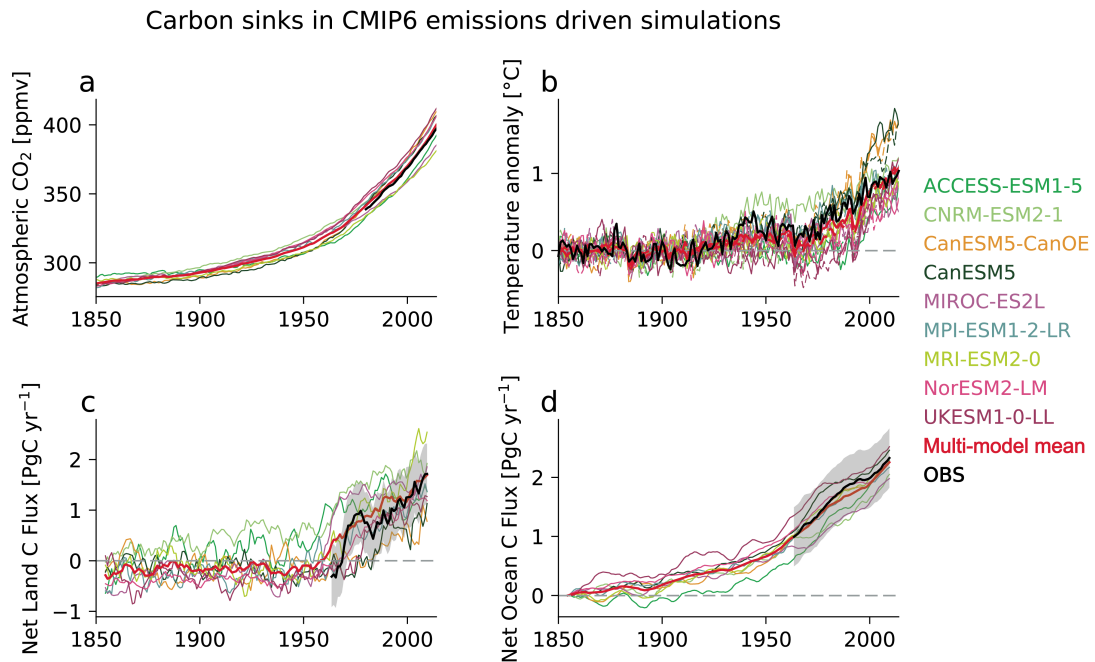


Figure 1.1: Model results for atmospheric CO₂, temperature anomaly, net land carbon flux and net ocean carbon flux from various models using Coupled Model Intercomparison Project Phase 6 (CMIP6) and observational data. The x-axis is years in all the plots. The black line represents the observational data, the red line is the mean of all the models used, and every other line is an individual model that can be determined using the colour coded legend in all plots. Figure 3.31 in [11].

marine carbon dioxide (mCDR) methods. One of these methods is known as ocean alkalinity enhancement (OAE). OAE works through the process of adding alkaline materials into the ocean in an effort to reduce the amount of CO_2 in the ocean. When the alkaline material dissolves in the ocean it causes the partial pressure of oceanic CO_2 to decrease. In order to restore a pressure equilibrium with the atmosphere the ocean would then absorb the atmospheric CO_2 above it until an equilibrium is reached.[14]. Since an alkalinity increase leads to reactions that accept protons the pH of the ocean will be increased, which also helps with reducing the increasing acidity of the ocean[14].

1.2 Motivation

A crucial aspect of any CDR method is known as monitoring, measuring, reporting, and verification (MMRV). This process is necessary as it allows for understanding of how effective the CDR method is. For OAE an important aspect for effective MMRV is knowing where the alkaline particles spread after initially being added to a body of water, as the drift of particles within the ocean will determine where OAE will occur. These particles are very difficult to actually track as they spread throughout the ocean as each individual particle is extremely small and will have its own path that must be monitored[8]. This would require equipment capable of detecting individual particles of the alkaline material to be covering a wide area of water, which would be extremely expensive and is an unrealistic method for MMRV to be conducted in OAE. In order to predict the trajectories of these particles ocean models must be used. Experimental methods of measuring ocean circulation such as surface drifters are not effective in determining particle trajectories as they have a much larger mass than the released particles will have, which will which will cause differences in their motion[7]. Hence, the results from these models are crucial as it is the only feasible way to obtain data about the trajectories and impact that adding millions of particles will have.

Before an ocean model can be used to predict the trajectories of particles it must first be verified to be accurate in modelling the features of the ocean without any added particles, such as the water velocity, salinity, and temperature. After an ocean model has been validated to give very similar results as field measurements of the ocean it can then be used for modelling particle trajectories. Since coastal regions are

extremely shallow they are more prone to instability in models, so in coastal ocean models it is especially important for these values to stay close to measured data. If the values in these regions varies from measured data the models results can rapidly increase and become nonphysical.

Previous studies have found that OAE will have a higher net reduction in atmospheric CO₂ levels when alkaline particles are introduced in coastal regions[2]. This project presents an ocean model of the Newfoundland Basin, which includes influences from the Labrador current, Gulf stream, as well as various surface and deep sea currents. First a model was developed for modelling of ocean circulation in this region. After this model was developed and tested there were simulations for particles added in the Conception Bay region and surrounding area. Once the particles are initially distributed in the region the model will predict their trajectories based on the surface currents for a short time. After some time the particles will sink below the ocean surface and their movement will no longer be effected by the surface currents, but by the circulation of the water beneath the ocean surface. The evolution of these particles can then be studied as the model progresses and the particles begin to spread out away from the initial region. The effects these particles have on CO₂ uptake and other environmental factors can then be determined.

In order for an accurate model to be created in the Newfoundland Basin, an ocean model that is designed for use in coastal regions must be used[16]. This project uses Regional Ocean Modeling System (ROMS) to develop the model. ROMS is designed for applications in coastal regions while also being capable of producing large-scale simulations. This allows for the development of a model that is very accurate in the areas near land, as well as in deeper regions further from land. Both of these features are crucial parts as the particles are initially released in shallow regions and then spread to deeper regions.

Chapter 2

Regional Ocean Modeling System (ROMS) features

2.1 Model Equations

ROMS is a three dimensional ocean model. The content found in this chapter is based on the information found on the ROMS wiki page [15]. The information here covers how the ocean model solves the problem at hand.

ROMS numerical solves the Navier-Stokes equation. The momentum balance in the x and y directions have the following forms:

$$\frac{\partial u}{\partial t} + \mathbf{v} \cdot \nabla u - fv = -\frac{\partial \phi}{\partial x} - \frac{\partial}{\partial z}(\overline{u'w'} - \nu \frac{\partial u}{\partial z}) + F_u + D_u \quad (2.1)$$

$$\frac{\partial v}{\partial t} + \mathbf{v} \cdot \nabla v + fu = -\frac{\partial \phi}{\partial y} - \frac{\partial}{\partial z}(\overline{v'w'} - \nu \frac{\partial v}{\partial z}) + F_v + D_v \quad (2.2)$$

where x, y are the horizontal coordinates, u, v are the x and y components of the velocity, \mathbf{v} is the velocity, D_u and D_v are the diffusive terms, F_u and F_v are the forcing terms, f is the Coriolis parameter, g is the acceleration due to gravity, and ν is the molecular viscosity. The over bar means the time averaged value and the primes mean the deviation from the mean value.

In the z-direction the hydrostatic approximation is used. This approximation assumes that the pressure at a certain level z is equal to the weight of the water column above it per unit area. This assumption is used as it is accurate to the

physical situation when the ratio of vertical (D) and horizontal (L) scales of motion is $D/L \ll 1$. The hydrostatic approximation greatly reduces the computational time required to the model and is given as follows:

$$\frac{\partial \phi}{\partial z} = -\frac{\rho g}{\rho_0} \quad (2.3)$$

where ϕ is the dynamic pressure, z is the vertical coordinate, ρ is the density of the water column, and ρ_0 is the density of water at the ocean surface.

ROMS models the ocean as an incompressible fluid. An incompressible fluid means that the time and spatial derivatives of its density is negligible small in the equation of mass conservation. The continuity equation for incompressible fluids is:

$$\frac{\partial u}{\partial x} + \frac{\partial v}{\partial y} + \frac{\partial w}{\partial z} = 0 \quad (2.4)$$

where w is the vertical velocity component.

The temperature and salinity are active tracers which affects the baroclinic pressure gradient in the momentum equation. The equation of these tracers is the advective-diffusion equation:

$$\frac{\partial C}{\partial t} + \mathbf{v} \cdot \nabla C = -\frac{\partial}{\partial z}(\overline{C'w'}) - \nu_\theta \frac{\partial C}{\partial z} + F_C + D_C \quad (2.5)$$

where F_C is the forcing term, D_C is the diffusive term, and ν_θ is the molecular diffusivity.

The equation of state in ROMS is:

$$\rho = \rho(T, S, P) \quad (2.6)$$

where T is temperature, S is salinity, and P is the total pressure. It determines the dependence of density from the temperature, salinity, and pressure.

The vertical turbulent fluxes, or Reynolds fluxes, of momentum and tracers are determined through the coefficients of turbulent mixing for momentum (K_M) and tracers (K_C) respectively:

$$\overline{u'w'} = -K_M \frac{\partial u}{\partial z} \quad (2.7)$$

$$\overline{v'w'} = -K_M \frac{\partial v}{\partial z} \quad (2.8)$$

$$\overline{C'w'} = -K_C \frac{\partial C}{\partial z} \quad (2.9)$$

where K_M and K_C are the vertical eddy viscosity and diffusivity terms.

2.2 Vertical coordinate system

ROMS uses a s-coordinate vertical coordinate system. It is a terrain-following coordinate system that allows for the correct representation of the bottom topography and bottom boundary conditions. Using these coordinates also allows a better resolution in the bottom boundary layer, while having more accurate results of pressure gradients near the surface[12]. The σ coordinate has a range of $-1 \leq \sigma \leq 0$, where $\sigma = 0$ at the ocean surface, and $\sigma = -1$ at the bottom surface. Inside of ROMS there are two different variations of this transformation. The one used in this study has the form:

$$z(x, y, \sigma, t) = \zeta(x, y, t) + [\zeta(x, y, t) + h(x, y)]S(x, y, \sigma) \quad (2.10)$$

where

$$S(x, y, \sigma) = \frac{h_c \sigma + h(x, y)C(\sigma)}{h_c + h(x, y)} \quad (2.11)$$

where $h(x, y)$ is the bottom depth, h_c is a positive value that controls the stretching, and $C(\sigma)$ is a stretching function. This transformation was used as it allows for layers near the surface in deeper regions to be further spaced out than in the other transformation, which improves stability.

Within ROMS there are also five different stretching functions available. Each stretching function is dimensionless, nonlinear, and monotonic. They also must be continuous and differentiable, or piecewise and differentiable with a smooth transition. All stretching functions define the σ coordinate as:

$$\sigma(k) = \begin{cases} \frac{k-N}{N}, & \text{at vertical W-points, } k = 0, \dots, N \\ \frac{k-N-0.5}{N}, & \text{at vertical } \rho \text{-points, } k = 1, \dots, N \end{cases} \quad (2.12)$$

The stretching function used in this model separates the top and bottom stretching

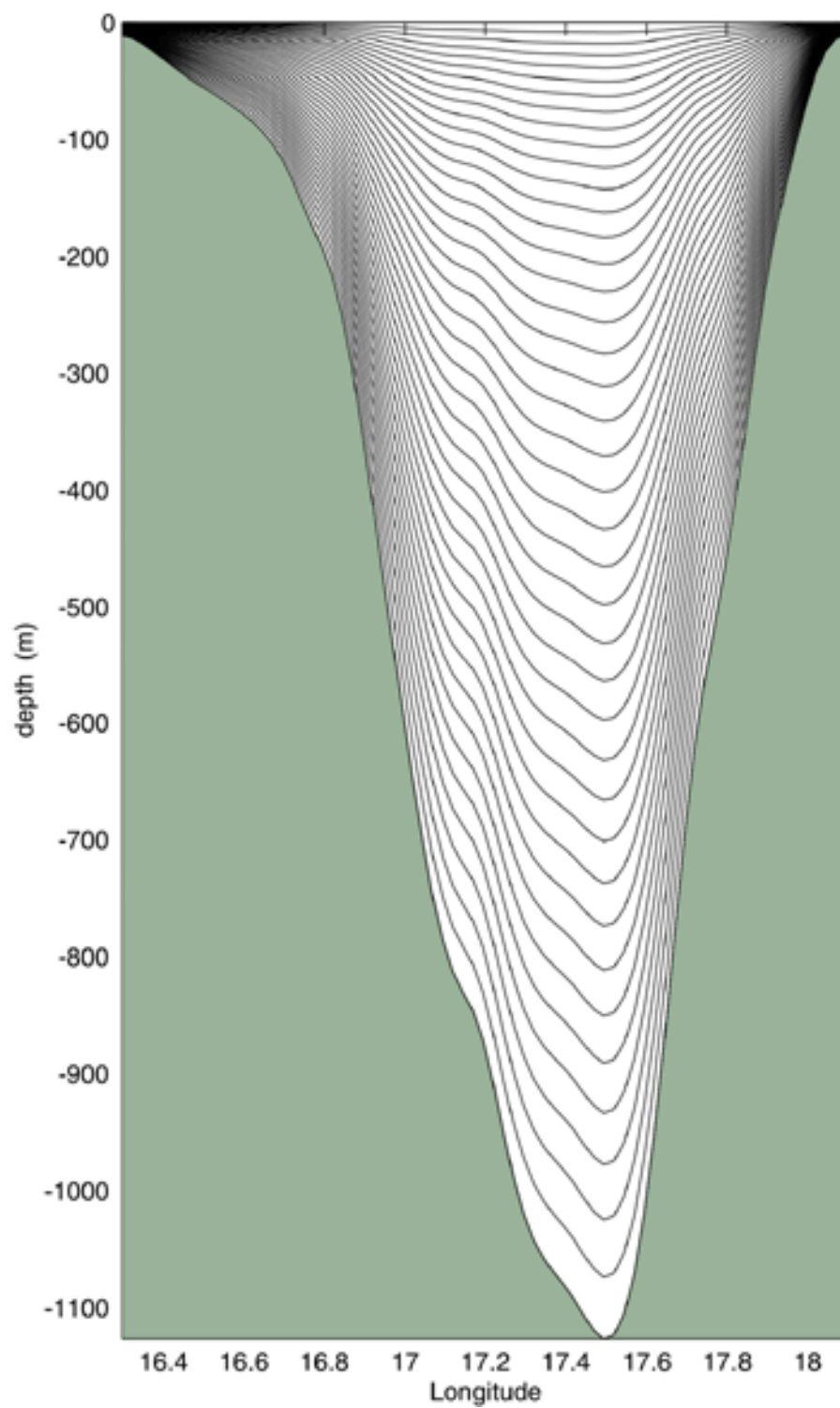


Figure 2.1: Terrain-following vertical coordinate. From ROMS wiki, February 29 2008, <https://www.myroms.org/wiki/File:vieste-dubrovnik.png>, obtained April 27, 2025.

into two separate functions with the forms:

$$C_{sur}(\sigma) = \begin{cases} \frac{1 - \cosh(\theta_s \sigma)}{\cosh(\theta_s) - 1}, & \text{for } \theta_s > 0 \\ -\sigma^2, & \text{for } \theta_s \leq 0 \end{cases} \quad (2.13)$$

$$C_{bot} = \frac{e^{\theta_B C_{sur}(\sigma)} - 1}{1 - e^{-\theta_B}} \quad (2.14)$$

where θ_S and θ_B are the surface and bottom control parameters respectively. For this functions they have the ranges $0 \leq \theta_s \leq 10$ and $0 \leq \theta_B \leq 4$. This stretching function was used as it is the setting suggested by ROMS.

2.3 Boundary conditions

The lateral boundary conditions determine the values of model variables at the lateral boundaries. The conditions at the closed boundaries normally determine no-normal flux of heat and salt and no-slip boundary condition for velocity. The conditions at open boundaries are defined as radiative boundary conditions. The radiative boundary conditions lets the disturbances generated inside the model domain to leave the domain without reflection.

ROMS equations and boundary conditions are written in general curvilinear orthogonal coordinates ξ and η are a new set of orthogonal coordinates.

$$1 = \phi_\xi \frac{\partial \phi}{\partial \xi} + \phi_\eta \frac{\partial \phi}{\partial \eta} \quad (2.15)$$

where

$$\phi_\xi = \frac{\frac{\partial \phi}{\partial \xi}}{\left(\frac{\partial \phi}{\partial \xi}\right)^2 + \left(\frac{\partial \phi}{\partial \eta}\right)^2} \quad (2.16)$$

$$\phi_\eta = \frac{\frac{\partial \phi}{\partial \eta}}{\left(\frac{\partial \phi}{\partial \xi}\right)^2 + \left(\frac{\partial \phi}{\partial \eta}\right)^2} \quad (2.17)$$

$$(2.18)$$

$$(dS)_\xi = \left(\frac{1}{m}\right) d\xi \quad (2.19)$$

$$(dS)_\eta = \left(\frac{1}{n}\right) d\eta \quad (2.20)$$

where ϕ is the value of an arbitrary variable, m and n are scaling factors that relate the arc length to the new coordinates.

In addition to the lateral boundary conditions, there is also a set of boundary conditions at the surface and bottom. The surface boundary conditions determine surface fluxes of momentum, heat and salt and the position of the ocean free surface:

$$K_M \frac{\partial u}{\partial z} = \tau_s^x(x, y, t) \quad (2.21)$$

$$K_M \frac{\partial v}{\partial z} = \tau_s^y(x, y, t) \quad (2.22)$$

$$K_C \frac{\partial C}{\partial z} = \frac{Q_C}{\rho_o} \quad (2.23)$$

$$w = \frac{\partial \zeta}{\partial t} \quad (2.24)$$

where τ_s is the surface wind shear stress, Q_C is the surface flux of scalars.

The bottom boundary conditions determine the bottom fluxes of momentum, heat and salt as well as the kinematics of the near-bottom ocean elements over the bottom topography $h(\eta, \xi)$:

$$K_M \frac{\partial u}{\partial z} = \tau_b^x(x, y, t) \quad (2.25)$$

$$K_M \frac{\partial v}{\partial z} = \tau_b^y(x, y, t) \quad (2.26)$$

$$K_C \frac{\partial C}{\partial z} = 0 \quad (2.27)$$

$$w = \mathbf{v} \cdot \nabla h \quad (2.28)$$

where τ_b is the bottom friction:

$$(\tau_b^x, \tau_b^y) = C_D(u, v)\sqrt{u^2 + v^2}$$

where C_D is an empirical friction coefficient.

The bottom flux of heat and salt is set to zero in these simulations. The bottom

heat flux, or geothermal flux, is nonzero, but its value normally small and not well known. Therefore, it is assumed that this flux is negligible for the purposes of this study.

2.4 Grid structure

ROMS uses an Arakawa C grid, which calculates the u and v velocity components and scalar value at different points on the staggered grid. The u component of velocity is calculated at the West and East grid point boundaries, the v component of velocity is calculated at the North and South grid point boundaries, and scalars are calculated in the center of each grid point, as shown 2.2. This grid structure is used because calculating each property at different points improves accuracy and stability.

ROMS also uses a staggered grid in the vertical direction. Some values are calculated at one vertical level, and the other values are calculated at the next level. In ROMS, the horizontal components of velocity and scalars are calculated at one level and the vertical velocity is calculated at the next layer, as shown in 2.3. This grid structure was used as it also improves stability and accuracy[18].

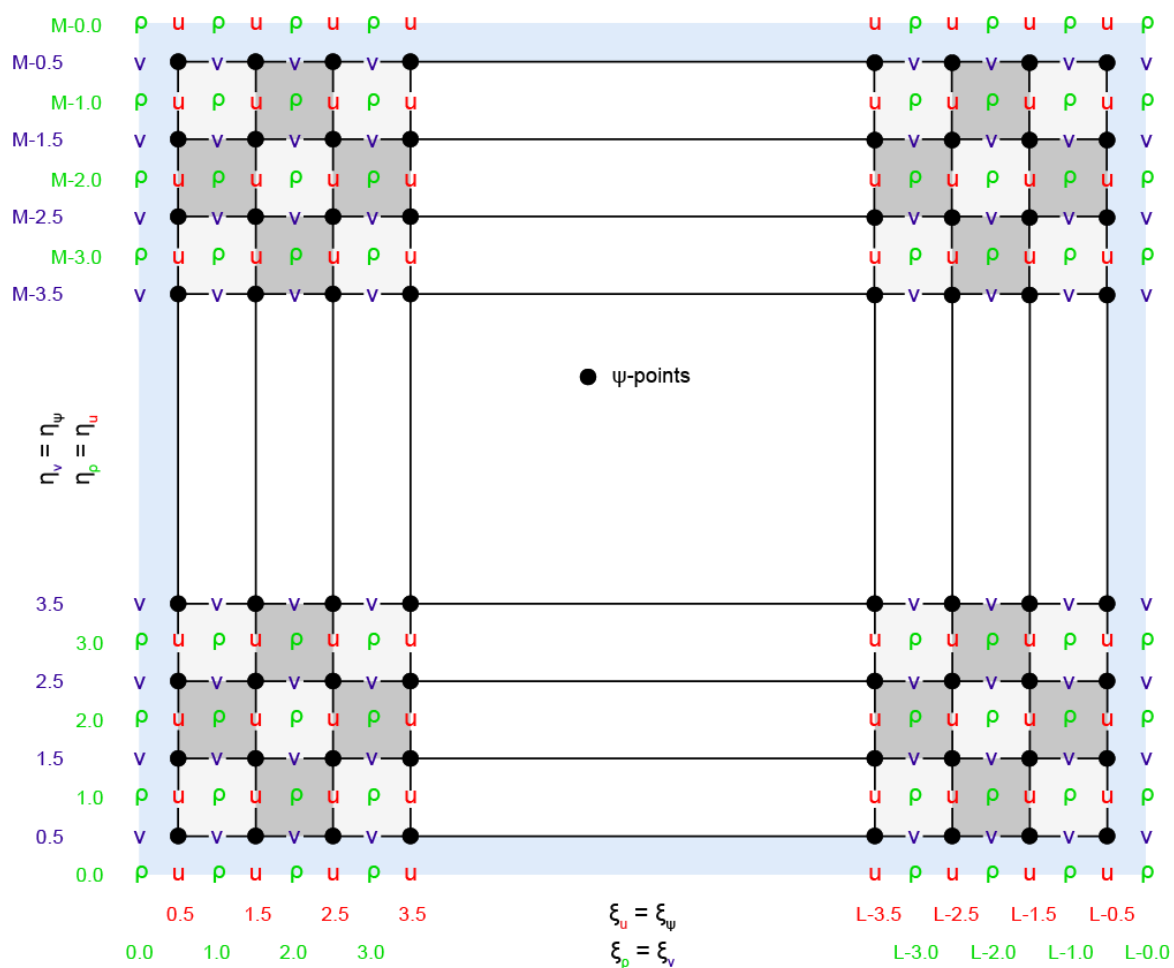


Figure 2.2: Arakaw C grid It shows where each value is calculated on each grid point. The u velocity component is calculated at the boundaries in the x direction, the v velocity component is calculated at the boundaries in the y direction, and all other values, denoted by ρ are calculated at the center of the cell. From ROMS wiki, May 6 2016, https://www.myroms.org/wiki/File:nesting_staggered_grid_rho_cells.png, obtained on April 23, 2025.

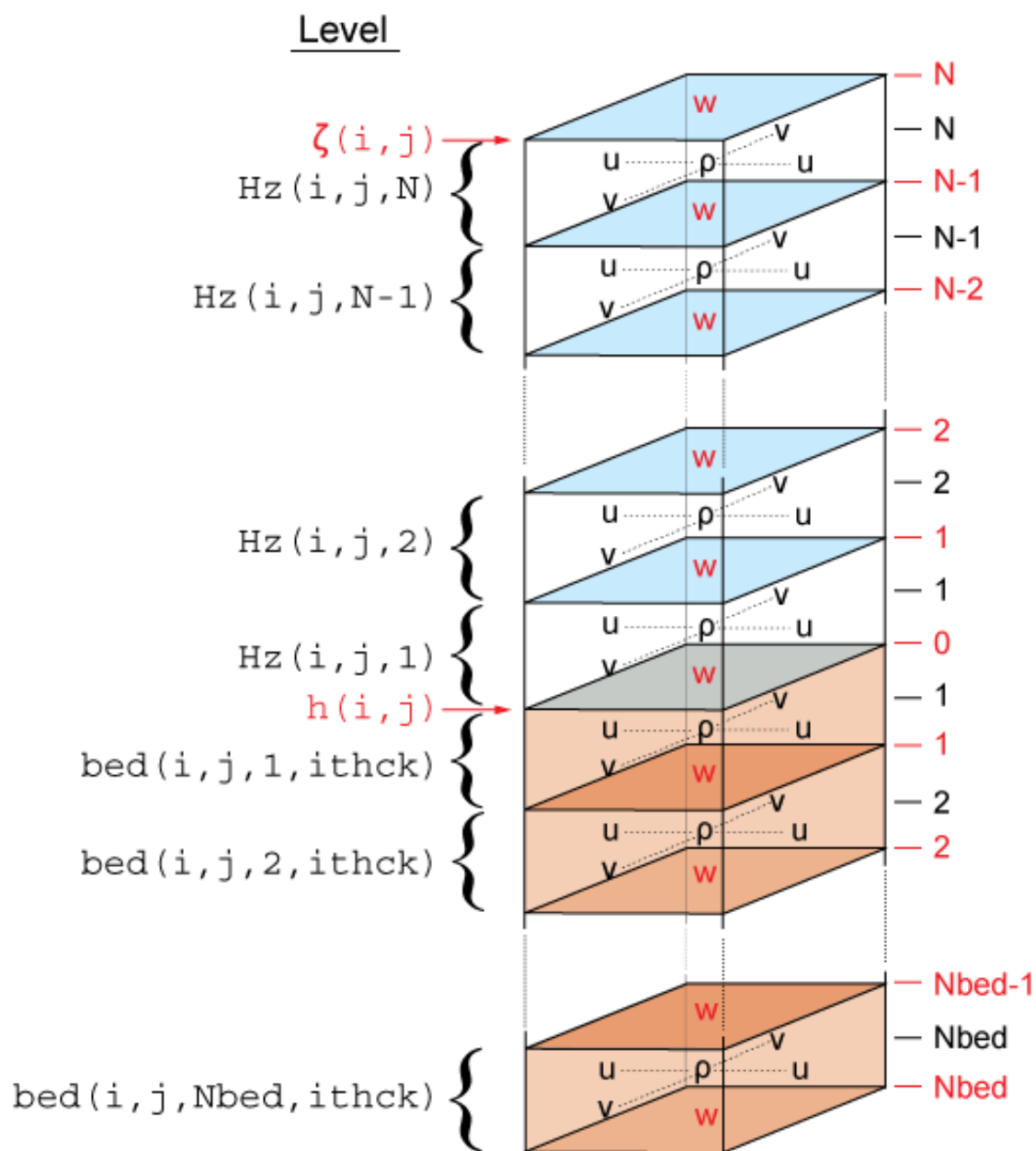


Figure 2.3: Staggered vertical grid used in ROMS. From ROMS wiki, March 7 2008, https://www.myroms.org/wiki/File:vertical_grid.png, obtained April 23, 2025.

Chapter 3

Model Implementation

3.1 Grid building

The first step in the model implementation is the generation the model domain and model topography. One way to this is ROMS is by using the MATLAB tool Grid-Builder (<https://austides.com/wp-content/uploads/GridBuilder-v0.99.pdf>). The grid used here has 470 grid points in the latitudinal direction and 390 in the longitudinal direction. This resulted in a resolution of 3km in both directions. The bottom topography is derived from General Bathymetric Chart of the Oceans (GEBCO) (<https://www.gebco.net/data-products/gridded-bathymetry-data>) bottom topography data set with 15 arc-second interval grid. This data for the bottom topography is shown in 3.1. The bathymetry was then smoothed by using spatial low-pass filter in order to improve stability of the model. The area includes a broad shelf known also as the Newfoundland Rise followed by steep continental slope. The highest depth in the region is ~ 3000 m. Key elements of the topography of the Newfoundland Rise are the Newfoundland Grand Banks, Flemish Cap and the narrow Flemish pass [13].

3.2 Atmospheric forcing

The surface boundary conditions are calculated by using atmospheric characteristics from an atmospheric reanalysis. The data is obtained from the European Centre for

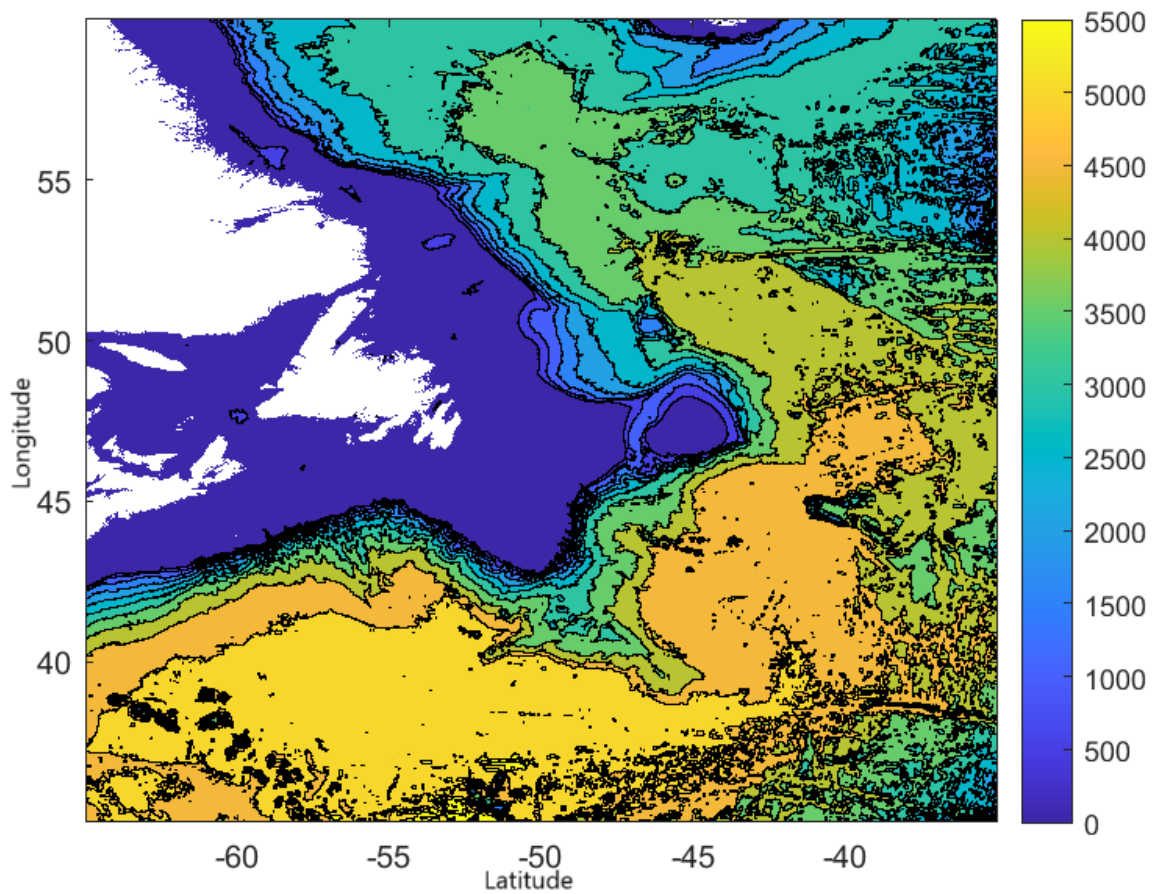


Figure 3.1: Bathymetry in the Newfoundland Basin and its surrounding region. The colour bar depicts ocean depth in units of meters.

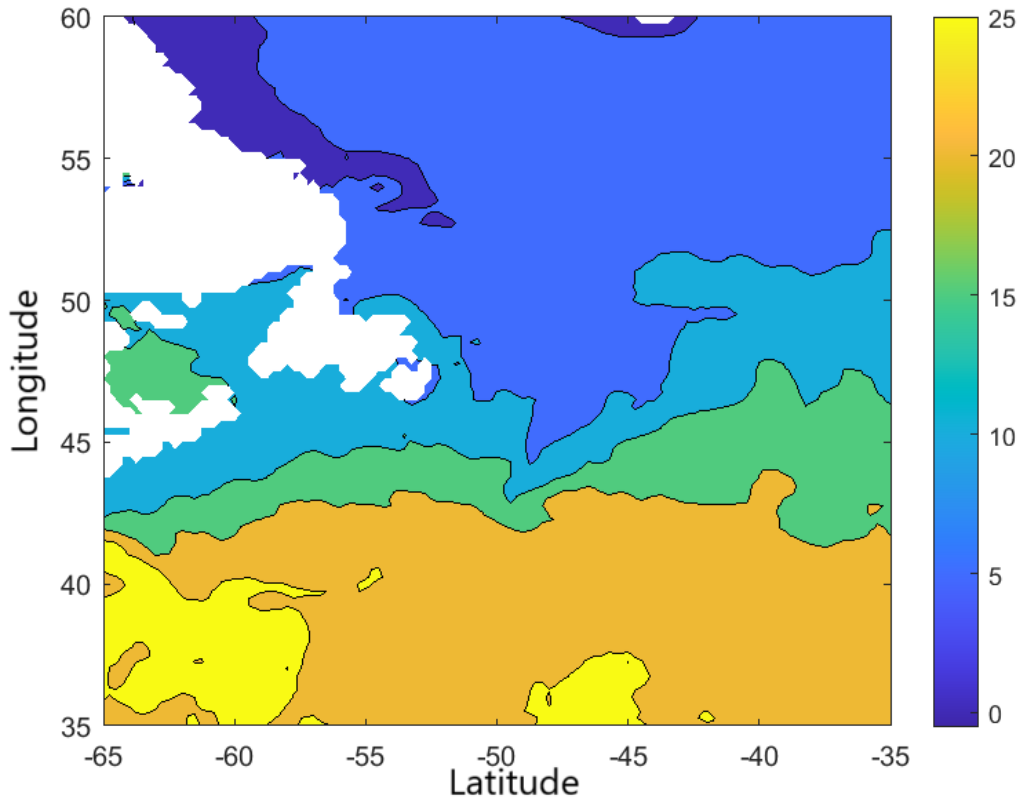


Figure 3.2: Sea surface temperature on July 1, 2020 at 12:00 p.m. Data is obtained from the dataset ERA5 hourly data on single levels from 1940 to present. The colour bar has units of $^{\circ}\text{C}$.

Medium-Range Weather Forecasts (ECMWF). The dataset used is the hourly ERA5 data on standard levels. 3.2 shows an example of an atmospheric characteristic used in calculating the surface fluxes, using sea surface temperature.

The surface atmospheric fluxes in ROMS are calculated by using the bulk formulation. It allows for calculation of fluxes by using the feedback from ocean model[1]. The equations using the bulk formulation are:

$$\tau = \rho C_D U \mathbf{u}_z \quad (3.1)$$

$$Q_H = \rho C_P C_H (\theta_z - T_S) U \quad (3.2)$$

$$E = \rho C_E (q_0 - q_z) U \quad (3.3)$$

$$Q_L = -L_v E \quad (3.4)$$

where:

τ is the surface wind stress

C_D is the bulk transfer coefficient for wind stress

U is the scalar wind speed

\mathbf{u}_z is the wind velocity vector at height z above the ocean surface

Q_H is turbulent flux of sensible heat

C_P is the heat capacity of moist air

C_H is the bulk transfer coefficient for sensible heat

θ_z is the potential temperature at height z

T_S is the potential temperature at the ocean surface

E is the evaporation

C_E is the bulk transfer coefficient for moisture

q_0 is specific humidity at the ocean surface

q_z is specific humidity at height z above the ocean surface

Q_L is turbulent flux of latent heat

L_v is the latent heat of vaporization.

3.3 Initial conditions

The initial condition for the model determines the ocean characteristics at the initial time step. The process of determining these characteristics is called model initialization and it is the first step in every model implementation. Usually, the initial conditions are calculated from a gridded observational data set or output from another model. Since the model grid differs from the grid of the data set, initialization requires interpolation in space and sometimes in time.

The dataset used here is an the Global Ocean Physics Reanalysis from the Copernicus Marine Service[3]. This dataset collects observational data and produces the daily mean for each characteristic. The initialization time is July 1, 2020. The initialized variables are the sea surface height (SSH) , water velocity, temperature, and salinity, as described by equations 2.1-2.9. Note that the SSH is not defined by these equations, as it is determined only by the data included in this dataset. The interpolated results for sea surface height, temperature, and salinity, are shown in figures

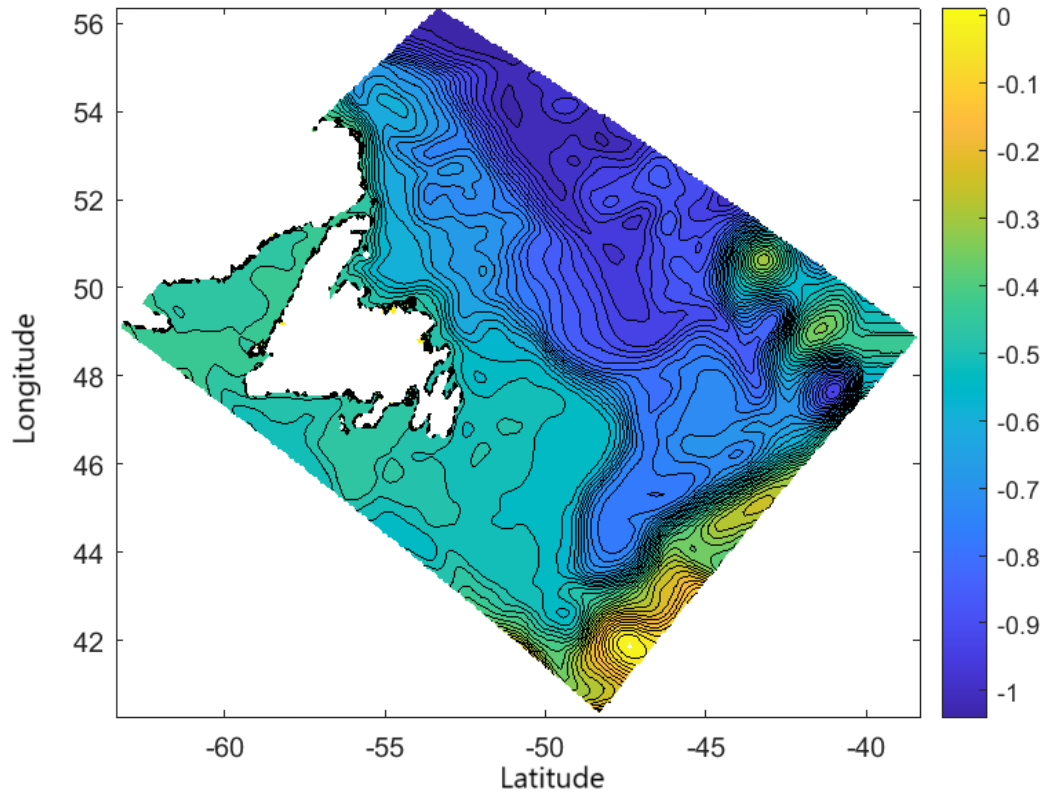


Figure 3.3: Initial condition for the SSH at 12:00 p.m. on July 1, 2020. The colour bar units are meters.

3.3, 3.4, and 3.5 respectively.

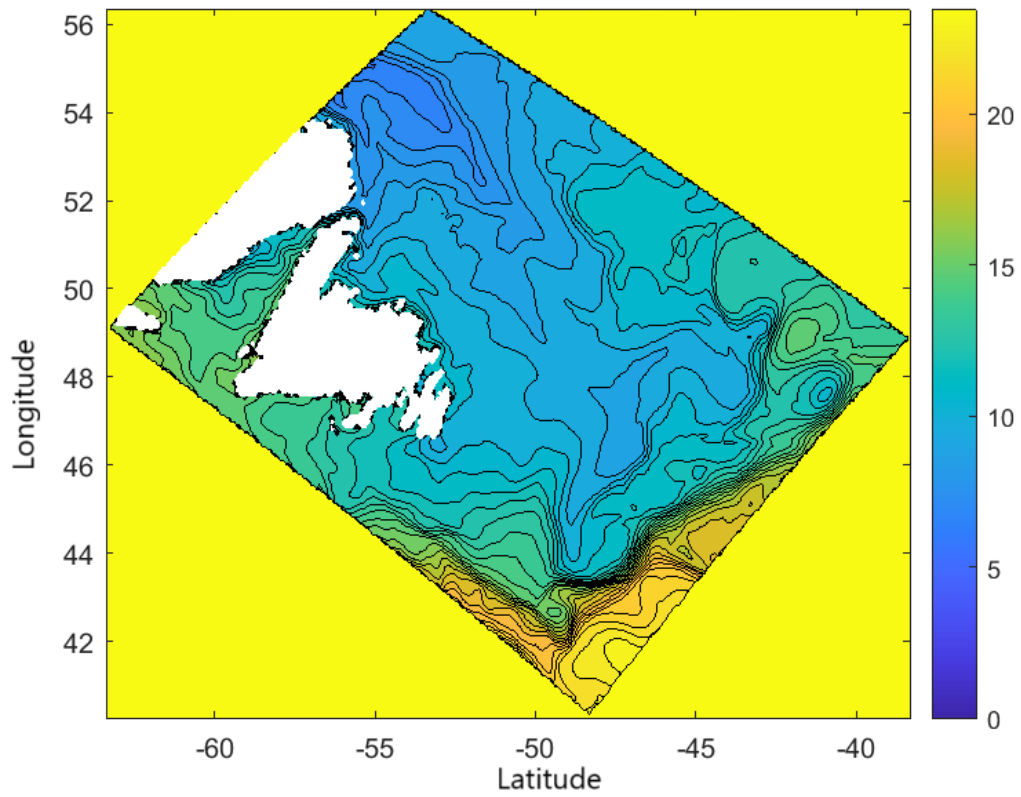


Figure 3.4: Initial condition for temperature at the ocean surface at 12:00 p.m on July 1, 2020. The colour bar units are $^{\circ}\text{C}$.

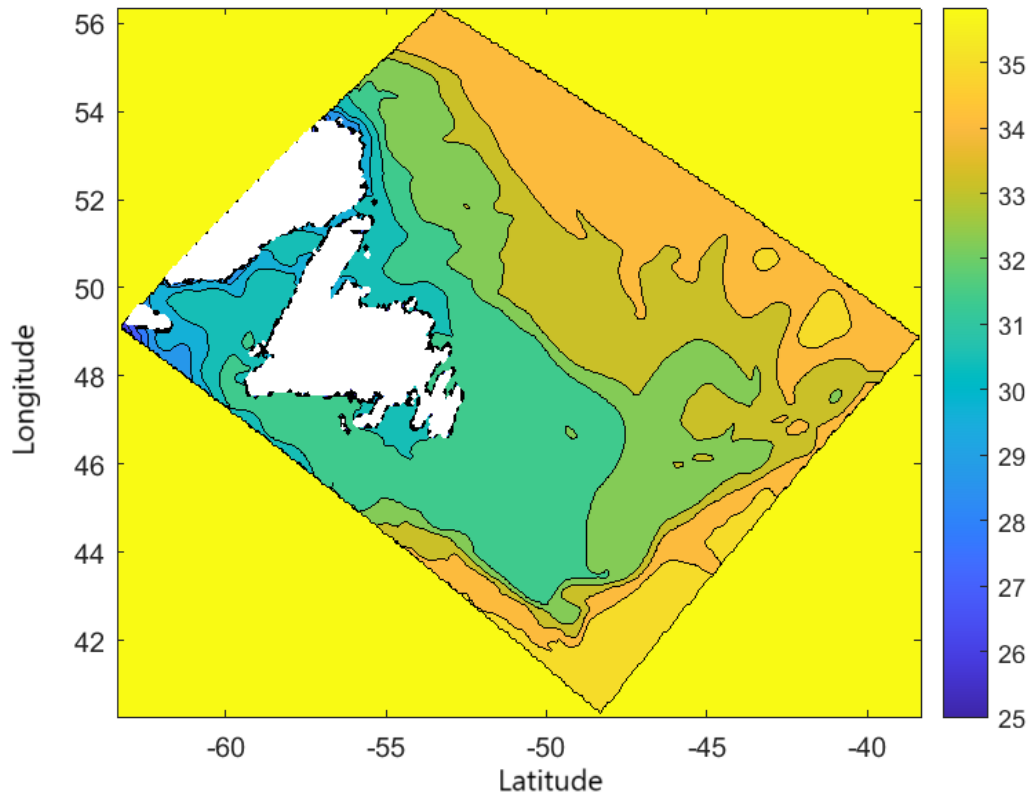


Figure 3.5: Initial condition for salinity at the ocean surface at 12:00 p.m on July 1, 2020. The colour bar represents the grams of salt per kilogram of water (g/kg).

3.4 Particle tracers

Particle trajectories in ROMS are dependant on the water velocities and ocean diffusivity. The equation that define the positions of particles are:

$$\mathbf{X}(t + \Delta t) = \mathbf{X}(t) + \mathbf{X}_{hydro} + \mathbf{X}_{vturb} + \mathbf{X}_{hturb} + \mathbf{X}_{behaviour} \quad (3.5)$$

where \mathbf{X} is the individual particles position vector, $\mathbf{X}(t + \Delta t)$ is the particles position vector after a time Δt , $\mathbf{X}(t)$ is the particles position at an earlier time t , \mathbf{X}_{hydro} is the particles displacement from the water velocity vector as calculated by ROMS, \mathbf{X}_{vturb} is a vertical displacement term calculated using vertical turbulent diffusivity, \mathbf{X}_{hturb} is a horizontal displacement term calculated using horizontal turbulent diffusivity, and $\mathbf{X}_{behaviour}$ is the displacement associated with sinking or rising of the particles[9].

Particles within ROMS can be added using internal input files. The input file chosen for this study releases the particles at the sea surface initially and allows them to sink after release. The number of particles released and the initial position was specified within the input file. The input file had two options for the release of particles. One option allowed for particles to be released over a wide distance but at one time, the other allowed particles to be released over a distance of time, but only in one fixed location. For this study the first option was used, to simulate particles being dumped instantaneously.

Chapter 4

Results

4.1 The sea surface height

SSH is the height of the ocean surface above a reference ocean surface level. The SSH is an important characteristic, which also determines the barotropic component of ocean pressure. In the rotating ocean, the SSH (barotropic pressure) is approximately balanced by the Coriolis Force, resulting in a geostrophic balance. As such, the SSH isolines are tangential to the geostrophic barotropic velocity and are indicative of the direction and strength of this velocity. The low negative values of the SSH in 3.3 show the part of the cyclonic flow known as the Subpolar Gyre. The high density of isolines along the west and south edges of the cyclonic gyre indicates the position of the Labrador Current. The high values of SSH in the southern part of the domain represent the North Atlantic Current, which brings warm, modified subtropical ocean waters northeastward. The broad area of the shelf (the Newfoundland Rise) is characterized by relatively homogeneous SSH.

Comparing 3.3 and 4.1, there is not much of a difference between the SSH between the beginning and end of July 2020. The changes in SSH during this period are due mainly to the non-stationary component of SSH driven by winds. During the summer period, these changes are small due to the relatively calm winds and are not remarkable in the distribution of SSH, which is dominated by the effects of the main large-scale currents.

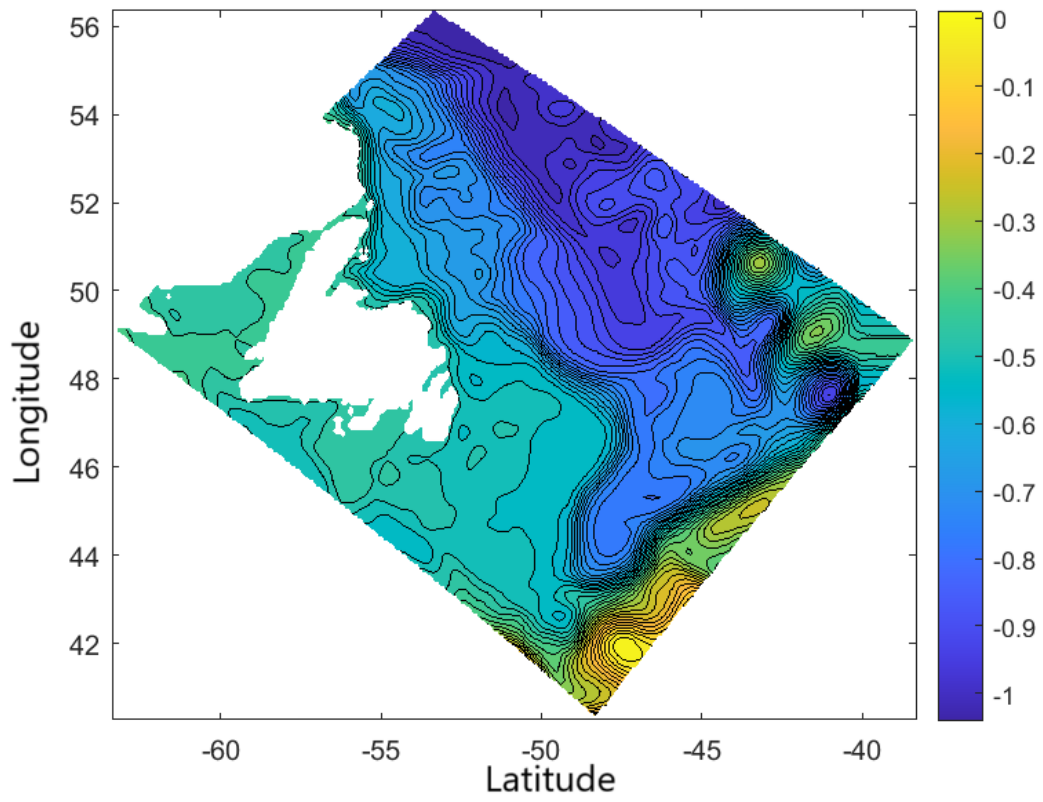


Figure 4.1: SSH at 12:00 p.m. on July 31, 2020. The colour bar units are meters.

4.2 The sea surface temperature

Like SSH, the sea surface temperature (SST) depends on the main currents and transports within the model domain. The SST shown in 4.2 shows the two major water masses in the model domain. The first one is the subpolar water mass with temperatures below 10°C . The Labrador Current transports this water mass southwestward. As this water spreads and mixes with the surrounding waters in the Newfoundland Basin, its temperature gradually increases. Comparing with the initial condition 3.4, we can observe that the core of the cold waters in the Labrador Sea becomes colder, and the gradient between these waters and the surrounding waters is more pronounced. This is an expected effect of the strengthening of the transport in the Labrador Current which is expected to be better resolved in the ROMS model than in the reanalysis due to the higher horizontal and vertical resolution.

There are also certain improvement in the representation of the warm modified subtropical waters in the southern part of the model domain after one month of simulation. The thermal front separating the warm subtropical waters from the subpolar waters becomes sharper. This is an expected impact of the improved transport by the North Atlantic Current due to higher model resolution in ROMS.

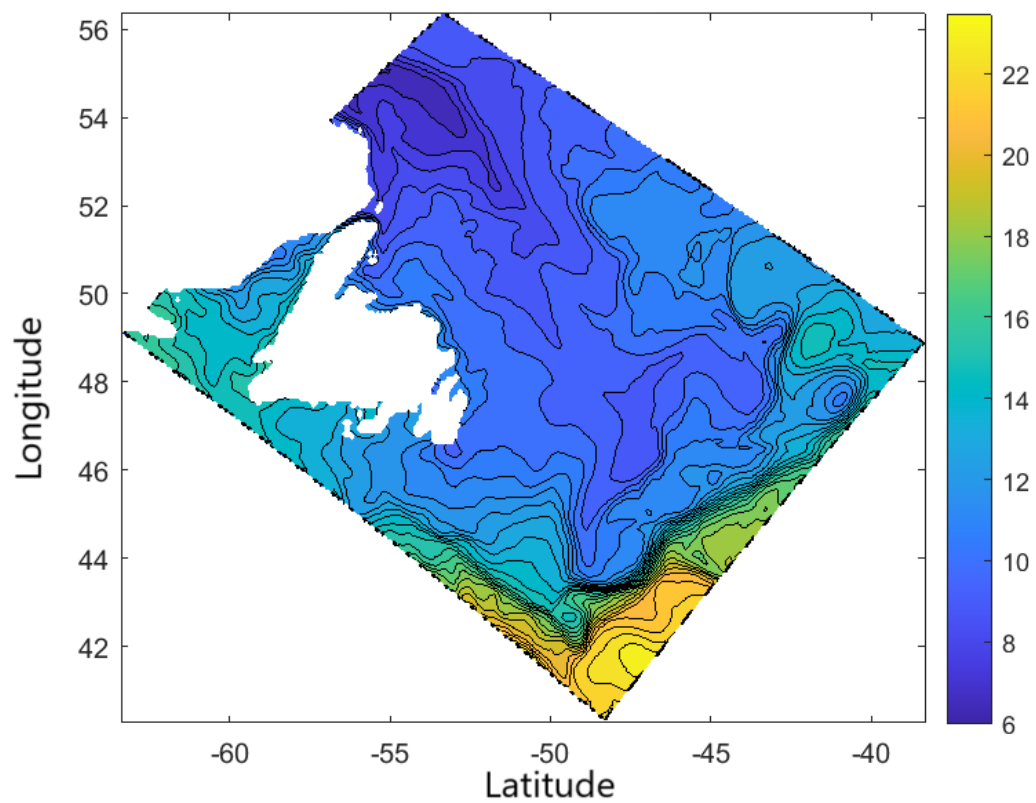


Figure 4.2: Sea surface temperature at 12:00 p.m. on July 31, 2020. The colour bar units are $^{\circ}\text{C}$.

4.3 The sea surface salinity

While the water masses observed in the sea surface salinity (SSS) distribution in 4.3 are the same as the SSS in 3.5, the SSS is more complex in 4.3 due to the impact of the coastal freshwater input. The ROMS implementation does not include freshwater input from the coastal regions. However, the significant effect on the freshwater input from the coastal areas comes from rivers like the Churchill River and Northwest River, which originate from parts of Labrador that are northern of the model domain. In this model step, this input affects the model solution through the boundary conditions. The near-coastal current transports this freshwater input, sometimes referred to as the coastal branch of the Labrador Current. The coastal branch separated from the coast near the east Newfoundland Coast and joins the main branch of the Labrador Current over the continental slope.

We also observe that the model strengthens the salinity gradients along the main currents, the Labrador Current and the North Atlantic Current. This change is expected and promising, as it suggests that the model will improve the ocean characteristics after initialization.

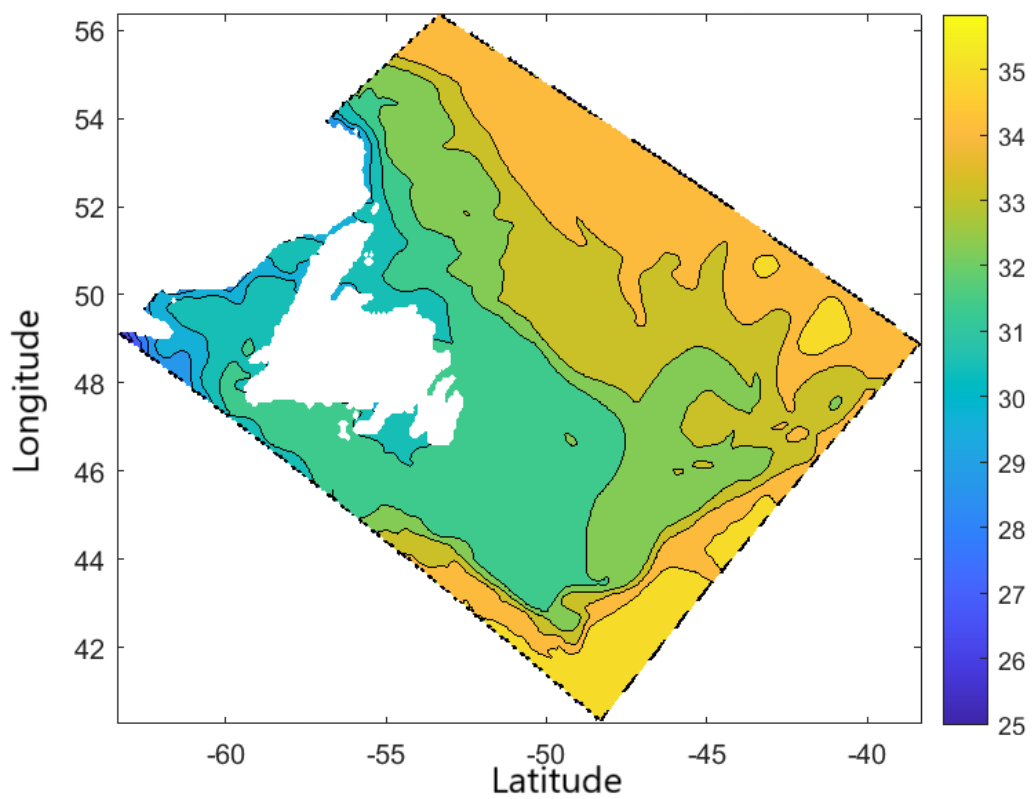


Figure 4.3: Sea surface salinity at 12:00 p.m. on July 31, 2020. The colour bar represents how many grams of salt there are per kilogram of water.

4.4 Particle trajectories

The simulation conducted in this study utilized 100 individual particles, all of which were dropped into the ocean at the surface at the initial time, July 1, 2020. The initial position of the particles ranged from a latitude of -52.6 to -52.1, and a longitude of 50.9 to 51.2. The particles then moved throughout the ocean for July. 4.4 shows the trajectory of these particles throughout the ocean during the month. The particles start in a square shape and then begin moving east. The initial region of the particle drops is around the area where the coastal branch of the Labrador Current separates from the coast and flows eastward. The particle followed the direction of the flow until they reached the main branch of the Labrador Current. Following the direction of the main branch, the particles moved southwest. While the particles follow the same general trend, the final positions are dispersed over a wider area than when they were initially released and don't form any uniform shape. The results here show the necessity of ocean modelling in the process of MMRV, as tracking each of these particles individually would require a lot of resources.

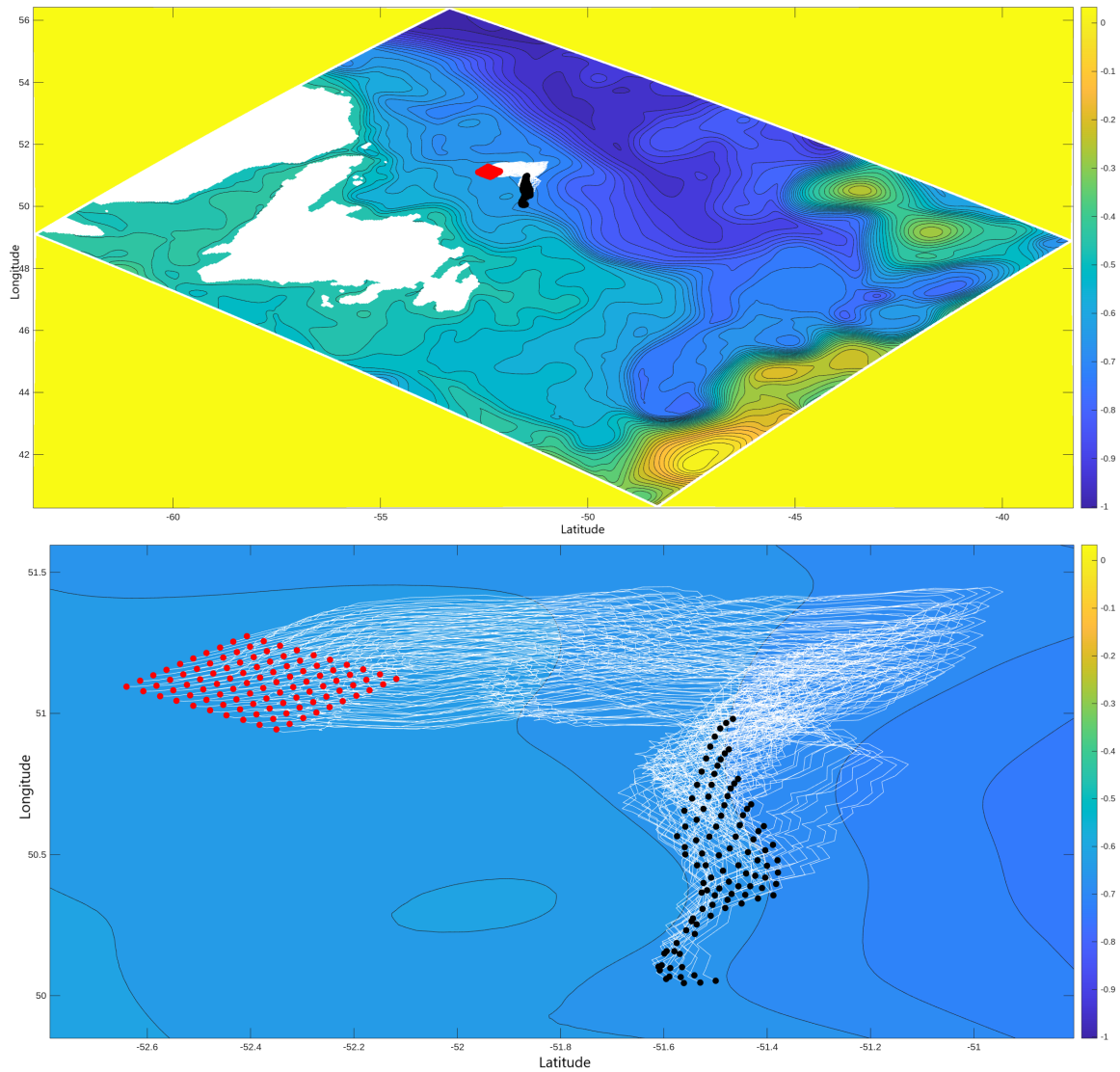


Figure 4.4: Trajectory of 100 particles during the month July 2020. The red dots represent the initial positions at 12:00 p.m. on July 1, 2020, the black dots denote the final positions projected onto the surface at 12:00 p.m. on July 31, 2020, and the white lines indicate the trajectories they followed throughout the month. The top figure shows the trajectories about the entire model domain. The bottom figure is zoomed in to show the individual trajectories. In both figures the x-axis is latitude and the y-axis is longitude. The top figure has a latitude range of -60 to -40 and a longitude range of 42 to 56. The bottom figures has a latitude range of -52.6 to -51 and a longitude range from 50 to 51.5. In both figures the colour bar is the SSH and ranges from 0 to -1.

Chapter 5

Conclusion

The work presented here highlighted how ocean models work and why they are necessary. Understanding the equations of ocean dynamics and how an ocean model works is crucial for comprehending the model results and addressing any issues that may arise during development. Using observational data of the atmosphere and ocean surface allows the model to provide results that are more accurate for the Earth's ocean. This is necessary to provide results that can be used to predict the effects that OAE could have on the region.

The work presented here is only the beginning of a much larger possible project. While the work presented here only spans July 2020, the model could be extended to run to the current time using observational data to compute the atmospheric forcing for longer time periods. The results from the model can then be compared with observational data to determine if they are accurate or not. If the results were not accurate, then other factors such as sea ice, tidal effects, and freshwater fluxes could be taken into consideration. After this is done it would be possible to extend the model to run past the present and be used as a predictive model.

The modelling of particle trajectories in this work was limited to a small number of particles released in a small area at one time. Future work could look at the effects of adding a larger number of particles in larger or smaller areas. A larger number of particles would yield more practical results than those presented in this study, as the number of particles added in reality is significantly larger than one hundred. They could also explore particles being steadily added over time at a single fixed point. This would also yield very practical results, as it would demonstrate how particles

move throughout the ocean when released from a pipe into the water, which is one of the most popular ideas for incorporating OAE[5].

The present work also demonstrates that modelling the effectiveness of alkaline materials in increasing ocean alkalinity, as described in [17] is possible by using ROMS. Further development and improvement of the present model set up will make possible studies of the effects of removing atmospheric CO₂ in the region. This would allow extending the model for longer periods and exploring different methods of particle addition. These future developments will make it possible to answer the question of how effective OAE would be if it were incorporated in the Newfoundland Basin, and which method of adding particles would be more effective.

Bibliography

- [1] G. Bonino, D. Iovino, and S. Masina. The bulk parameterizations of turbulent air–sea fluxes in NEMO4: the origin of sea surface temperature differences in a global model study. *Geoscientific Model Development*, 15:6873–6889, 2022.
- [2] D. J. Burt, F. Fröb, and T. Ilyina. The sensitivity of the marine carbonate system to regional ocean alkalinity enhancement. *Frontiers in Climate*, 3:624075, 2021.
- [3] *Global Ocean Physics Reanalysis. E.U. Copernicus Marine Service Information (CMEMS). Marine Data Store (MDS). DOI: 10.48670/moi-00021 (Accessed on 23-Jul-2024).*
- [4] S. C. Doney, W. H. Wolfe, D. C. McKee, and J. G. Fuhrman. The science, engineering, and validation of marine carbon dioxide removal and storage. *Annual Review of Marine Science*, 17:55–81, 2025.
- [5] K. Fennel, M. C. Long, C. Algar, B. Carter, D. Keller, A. Laurent, M. J. P., R. Musgrave, A. Oschlies, J. Ostiguy, J. B. Palter, and D. B. Whitt. Modelling considerations for research on ocean alkalinity enhancement (OAE). *State of the Planet*, 2:9, 2023.
- [6] J. Fuhrman, C. Bergero, M. Weber, S. Monteith, F. M. Wang, A. F. Clarens, S. C. Doney, W. Shobe, and H. McJeon. Diverse carbon dioxide removal approaches could reduce impacts on the energy–water–land system. *Nature Climate Change*, 4:341–350, 2023.
- [7] J. Furnans, J. Imberger, and B. R. Hodges. Including drag and inertia in drifter modelling. *Environmental Modelling and Software*, 23:714–728, 2008.
- [8] D. T. Ho, L. Bopp, J. B. Palter, M. C. Long, P. W. Boyd, G. Neukermans, and L. T. Bach. Monitoring, reporting, and verification for ocean alkalinity enhancement. *State of the Planet*, 2:12, 2023.
- [9] E. J. Hunter, H. L. Fuchs, J. L. Wilkin, G. P. Gerbi, R. J. Chant, and J. C. Garwood. ROMSpath v1.0: offline particle tracking for the regional ocean modeling system (ROMS). *Geoscientific Model Development*, 15:4297–4311, 2022.

- [10] IPCC. 2023: Summary for Policymakers. In: Climate Change 2023: Synthesis Report. Contribution of Working Groups I, II and III to the Sixth Assessment Report of the Intergovernmental Panel on Climate Change [Core Writing Team Lee, H. and Romero, J. (eds.)]. IPCC, Geneva, Switzerland, pp. 1-34, doi:10.59327/IPCC/AR6-9789291691647.001.
- [11] IPCC. IPCC, 2021: Climate Change 2021: The Physical Science Basis. Contribution of Working Group I to the Sixth Assessment Report of the Intergovernmental Panel on Climate Change [Masson-Delmotte, V., P. Zhai, A. Pirani, S.L. Connors, C. Péan, S. Berger, N. Caud, Y. Chen, L. Goldfarb, M.I. Gomis, M. Huang, K. Leitzell, E. Lonnoy, J.B.R. Matthews, T.K. Maycock, T. Waterfield, O. Yelekçi, R. Yu, and B. Zhou (eds.)]. Cambridge University Press, Cambridge, United Kingdom and New York, NY, USA, In press, doi:10.1017/9781009157896.
- [12] L. K. Kantha and C. A. Clayson. *Numerical Models of Oceans and Oceanic Processes*. Academic press, 2000.
- [13] C. Mertens, M. Rhein, M. Walter, C. W. Böning, E. Behrens, D. Kieke, R. Steinfeldt, and U. Stöber. Circulation and transports in the newfoundland basin, western subpolar north atlantic. *Journal of Geophysical Research: Oceans*, 11:7772–7793, 2014.
- [14] A. Oschlies, L. T. Bach, R. E. M. Rickaby, T. Statterfield, R. Webb, and J. Gattuso. Climate targets, carbon dioxide removal, and the potential role of ocean alkalinity enhancement. *State of the Planet*, 2:2, 2023.
- [15] *Regional Ocean Modeling System (ROMS) (n.d.)*. Wikiroms. Myroms. Retrieved April 22, 2025, from https://www.myroms.org/wiki/Documentation_Portal.
- [16] A. F. Shchepetkin and J. C. McWilliams. The regional oceanic modeling system (ROMS): a split-explicit, free-surface, topography-following-coordinate oceanic model. *Ocean Modelling*, 4:347–404, 2005.
- [17] H. Wang, D. J. Pilcher, K. A. Kearney, J. N. Cross, O. M. Shugart, M. D. Eisaman, and B. R. Carter. Simlated impact of ocean alkalinity enhancement on atmospheric CO₂ removal in the bering sea. *Earth’s Future*, 11, 2022.
- [18] L. Yang, H. Yan, and H. Liu. An optimal implicit staggered-grid finite-difference scheme based on the modified taylor-series expansion with minimax approximation method for elastic modeling. *Journal of Applied Geophysics*, 138:161–171, 2017.

Appendix A

Alternate formulations of equations of ocean dynamics

A.1 Using sigma coordinates

The equations of motion described in section 2.1 can also be described using the σ vertical coordinate system described in section 2.2. The content in this appendix is also based on information available at [15]. The equations become much more complicated using this formulation. The vertical grid thickness is described as $H_z = \frac{\partial z}{\partial \sigma}$. The equations in this coordinate system become:

$$\frac{\partial u}{\partial t} - fv + \mathbf{v} \cdot \nabla u = -\frac{\partial \phi}{\partial x} - \left(\frac{g\rho}{\rho_o}\right) \frac{\partial z}{\partial x} - g \frac{\partial \zeta}{\partial x} + \frac{1}{H_z} \frac{\partial}{\partial \sigma} \left[\frac{(K_m + \nu)}{H_z} \frac{\partial u}{\partial \sigma} \right] + F_u + D_u \quad (\text{A.1})$$

$$\frac{\partial v}{\partial t} - fu + \mathbf{v} \cdot \nabla v = -\frac{\partial \phi}{\partial y} - \left(\frac{g\rho}{\rho_o}\right) \frac{\partial z}{\partial y} - g \frac{\partial \zeta}{\partial y} + \frac{1}{H_z} \frac{\partial}{\partial \sigma} \left[\frac{(K_m + \nu)}{H_z} \frac{\partial v}{\partial \sigma} \right] + F_v + D_v \quad (\text{A.2})$$

$$\frac{\partial C}{\partial t} + \mathbf{v} \cdot \nabla C = \frac{1}{H_z} \frac{\partial}{\partial \sigma} \left[\frac{(K_C + \nu)}{H_z} \frac{\partial C}{\partial \sigma} \right] + F_C + D_C \quad (\text{A.3})$$

Equations A.1 and A.2 are the momentum balance equations in the x and y directions, and A.3 is the momentum balance for scalar tracers.

$$\frac{\partial \phi}{\partial \sigma} = \left(\frac{-gH_z \rho}{\rho_o} \right) \quad (\text{A.4})$$

Is the momentum balance in the vertical direction. It uses the same hydrostatic approximation that was described in section 2.1.

$$\rho = \rho(T, S, P) \quad (\text{A.5})$$

Is the equation of state, which is unchanged from the formulation in Cartesian coordinates.

$$\frac{\partial H_z}{\partial t} + \frac{\partial(H_z u)}{\partial x} + \frac{\partial(H_z v)}{\partial y} + \frac{\partial(H_z \Omega)}{\partial \sigma} = 0 \quad (\text{A.6})$$

Is the continuity equation, which still applies in this formulation. Where:

$$\mathbf{v} = (u, v, \Omega)$$

$$\nabla \cdot \mathbf{v} = u \frac{\partial}{\partial x} + v \frac{\partial}{\partial y} + \Omega \frac{\partial}{\partial \sigma}$$

ν is the molecular viscosity

K_m and K_C are the vertical eddy viscosity and diffusivity respectively.

F and D are the friction and damping in each direction.

The vertical velocity in the σ coordinate system is:

$$\Omega(x, y, \sigma, t) = \frac{1}{H_z} \left[w - \frac{z+h}{\zeta+h} \frac{\partial \zeta}{\partial t} - u \frac{\partial z}{\partial x} - v \frac{\partial z}{\partial y} \right] \quad (\text{A.7})$$

and

$$w = \frac{\partial z}{\partial t} + u \frac{\partial z}{\partial x} + v \frac{\partial z}{\partial y} + \Omega H_z \quad (\text{A.8})$$

In this coordinate system the vertical boundary conditions are:

At the top ($\sigma = 0$):

$$\left(\frac{K_m}{H_z} \right) \frac{\partial u}{\partial \sigma} = \tau_s^x(z, y, t) \quad (\text{A.9})$$

$$\left(\frac{K_m}{H_z} \right) \frac{\partial v}{\partial \sigma} = \tau_s^y(x, y, t) \quad (\text{A.10})$$

$$\left(\frac{K_C}{H_z} \right) \frac{\partial C}{\partial \sigma} = \frac{Q_C}{\rho_o c_p} \quad (\text{A.11})$$

$$\Omega = 0 \quad (\text{A.12})$$

At the bottom ($\sigma = -1$):

$$\left(\frac{K_m}{H_z}\right) \frac{\partial u}{\partial \sigma} = \tau_b^x(x, y, t) \quad (\text{A.13})$$

$$\left(\frac{K_m}{H_z}\right) \frac{\partial v}{\partial \sigma} = \tau_b^y(x, y, t) \quad (\text{A.14})$$

$$\left(\frac{K_C}{H_z}\right) \frac{\partial C}{\partial \sigma} = 0 \quad (\text{A.15})$$

$$\Omega = 0 \quad (\text{A.16})$$

A.2 Using curvilinear coordinates

The equations can also be described using the general curvilinear coordinates that were introduced in section 2.3. The velocity components in this coordinate system are $\mathbf{u} \cdot \hat{\xi}$ and $\mathbf{v} \cdot \hat{\eta}$. In this formulation the equations are as follows:

$$\begin{aligned} & \frac{\partial}{\partial t} \left(\frac{H_z u}{mn}\right) + \frac{\partial}{\partial \xi} \left(\frac{H_z u^2}{n}\right) + \frac{\partial}{\partial \eta} \left(\frac{H_z uv}{m}\right) + \frac{\partial}{\partial \sigma} \left(\frac{H_z u \Omega}{mn}\right) - \left[\left(\frac{f}{mn}\right) + v \frac{\partial}{\partial \xi} \left(\frac{1}{n}\right) - u \frac{\partial}{\partial \eta} \left(\frac{1}{m}\right) \right] H_z u \\ & = - \left(\frac{H_z}{n}\right) \left(\frac{\partial \phi}{\partial \xi} + \frac{g\rho}{\rho_o} \frac{\partial z}{\partial \xi} + g \frac{\partial \zeta}{\partial \xi}\right) + \frac{1}{mn} \frac{\partial}{\partial \sigma} \left[\frac{(K_m + \nu)}{H_z} \frac{\partial u}{\partial \sigma} \right] + \frac{H_z}{mn} (F_u + D_u) \end{aligned} \quad (\text{A.17})$$

$$\begin{aligned} & \frac{\partial}{\partial t} \left(\frac{H_z v}{mn}\right) + \frac{\partial}{\partial \xi} \left(\frac{H_z uv}{n}\right) + \frac{\partial}{\partial \eta} \left(\frac{H_z v^2}{m}\right) + \frac{\partial}{\partial \sigma} \left(\frac{H_z v \Omega}{mn}\right) + \left[\left(\frac{f}{mn}\right) + v \frac{\partial}{\partial \xi} \left(\frac{1}{n}\right) - u \frac{\partial}{\partial \eta} \left(\frac{1}{m}\right) \right] H_z v \\ & = \left(\frac{H_z}{m}\right) \left(\frac{\partial \phi}{\partial \eta} + \frac{g\rho}{\rho_o} \frac{\partial z}{\partial \eta} + g \frac{\partial \zeta}{\partial \eta}\right) + \frac{1}{mn} \frac{\partial}{\partial \sigma} \left[\frac{(K_m + \nu)}{H_z} \frac{\partial v}{\partial \sigma} \right] + \frac{H_z}{mn} (F_v + D_v) \end{aligned} \quad (\text{A.18})$$

Equations A.17-A.19 are the momentum transfer directions in the x, y, and z directions respectively. The momentum balance in the z direction still uses the hydrostatic approximation.

$$\begin{aligned} & \frac{\partial}{\partial t} \left(\frac{H_z C}{mn}\right) + \frac{\partial}{\partial \xi} \left(\frac{H_z u C}{n}\right) + \frac{\partial}{\partial \eta} \left(\frac{H_z v C}{m}\right) + \frac{\partial}{\partial \sigma} \left(\frac{H_z \Omega C}{mn}\right) \\ & = \frac{1}{mn} \frac{\partial}{\partial \sigma} \left[\frac{(K_m + \nu)}{H_z} \frac{\partial C}{\partial \sigma} \right] + \frac{H_z}{mn} (F_C + D_C) \end{aligned} \quad (\text{A.19})$$

Is the momentum balance for scalar tracers.

$$\rho = \rho(T, S, P) \quad (\text{A.20})$$

Is the equation of state, which is the same in all coordinate systems.

$$\frac{\partial \phi}{\partial \sigma} = - \left(\frac{g H_z \rho}{\rho_o} \right) \frac{\partial}{\partial t} \left(\frac{H_z}{mn} \right) + \frac{\partial}{\partial \xi} \left(\frac{H_z u}{n} \right) + \frac{\partial}{\partial \eta} \left(\frac{H_z v}{m} \right) + \frac{\partial}{\partial \sigma} \left(\frac{H_z \Omega}{mn} \right) = 0 \quad (\text{A.21})$$

Is the continuity equation, which remains the same in any coordinate system as the ocean is modelled as incompressible in all systems.

The boundary conditions remain the same in this transformation as what was shown in appendix A.1

Appendix B

Other stretching functions for terrain following vertical coordinates in ROMS

There are 4 alternate stretching functions that can be used inside of ROMS that were not used in this study. These functions are shown below in equations B.1 - B.4.

$$C(\sigma) = (1 - \theta_B) \frac{\sinh \theta_s \sigma}{\sinh \theta_s} + \theta_B \left[\frac{\tanh(\theta_s + \frac{1}{2})}{2 \tanh(\frac{1}{2} \theta_s)} - \frac{1}{2} \right] \quad (\text{B.1})$$

where $0 < \theta_s \leq 20$ and $0 \leq \theta_B \leq 1$

$$C(\sigma) = \mu C_{sur}(\sigma) + (1 - \mu) C_{bot}(\sigma) \quad (\text{B.2})$$

Where:

$$C_{sur}(\sigma) = \frac{1 - \cosh(\theta_s \sigma)}{\cosh \theta_s - 1}, \text{ where } \theta_s > 0$$

$$C_{bot}(\sigma) = \frac{\sinh[\theta_B(\sigma + 1)]}{\sinh(\theta_B)}, \text{ where } \theta_B > 0$$

$$\mu = (\sigma + 1)^\alpha \left[1 + \frac{\alpha}{\beta} (1 - (\alpha + 1)^\beta) \right]$$

here α and β are nondimensional scale factors.

$$C(\sigma) = \mu C_{bot}(\sigma) + (1 - \mu)C_{sur}(\sigma) \quad (\text{B.3})$$

Where:

$$C_{sur}(\sigma) = -\frac{\log [\cosh (\gamma|\sigma|^{\theta_s})]}{\log [\cosh (\gamma)]}$$

$$C_{bot}(\sigma) = \frac{\log [\cosh (\gamma(\sigma+1)^{\theta_B})]}{\log [\cosh (\gamma)]} - 1$$

$$\mu = \frac{1}{2} \left[1 - \tanh \left(\gamma \left(\sigma + \frac{1}{2} \right) \right) \right]$$

γ is a scale factor for the hyperbolic functions, with a typical value of $\gamma = 3$

The last transformation uses the same equations for $C_{sur}(\sigma)$ and $C_{bot}(\sigma)$ as the stretching function that was used in our study (see equations 2.13 and 2.14). However, it redefines the σ coordinate as follows:

$$\sigma(k) = \begin{cases} \frac{-k^2 - 2kN + k + N^2 - N}{N^2 - N} - \frac{1}{100} \frac{k^2 - kN}{1 - N}, & \text{at vertical W-points, } k = 0, \dots, N \\ \frac{-(k-0.5)^2 - 2(k-0.5)N + (k-0.5) + N^2 - N}{N^2 - N} - \frac{1}{100} \frac{(k-0.5)^2 - (k-0.5)N}{1 - N}, & \text{at vertical } \rho\text{-points, } k = 1, \dots, N \end{cases} \quad (\text{B.4})$$

Appendix C

Vertical mixing parameters

One of the most common mixing schemes is Mellor-Yamada 2.5. It uses two equations, one for kinetic energy, and another that uses kinetic energy times a length scale. The turbulent kinetic energy equation is given by:

$$\frac{D}{Dt} \left(\frac{q^2}{2} \right) - \frac{\partial}{\partial z} \left[kq \frac{\partial}{\partial z} \left(\frac{q^2}{2} \right) \right] = P_s + P_b + \xi_d \quad (\text{C.1})$$

Here P_s is the shear production, P_b is the buoyant production, and ξ_d is the dissipation of kinetic energy. $P_s = K_m [(\frac{\partial u}{\partial z})^2 + (\frac{\partial v}{\partial z})^2]$, $P_b = -K_s N^2$, $\xi_d = \frac{q^3}{B_1 l}$, where B_1 is a constant set to 16.6. $\frac{D}{Dt}$ is the material derivative, defined as:

$$\frac{D}{Dt} = \frac{\partial}{\partial t} + u \frac{\partial}{\partial x} + v \frac{\partial}{\partial y} + w \frac{\partial}{\partial z} \quad (\text{C.2})$$

Adding a biharmonic diffusion term D_q in the turbulent kinetic energy equation changes the equation to:

$$\begin{aligned} \frac{\partial}{\partial t} \left(\frac{H_z q^2}{mn} \right) + \frac{\partial}{\partial \xi} \left(\frac{H_z u q^2}{n} \right) + \frac{\partial}{\partial \eta} \left(\frac{H_z v q^2}{m} \right) + \frac{\partial}{\partial s} \left(\frac{H_z \Omega q^2}{mn} \right) - \frac{\partial}{\partial s} \left(\frac{K_q}{mn H_z} \frac{\partial q^2}{\partial s} \right) = \\ \frac{2H_z K_m}{mn} \left[\left(\frac{\partial u}{\partial z} \right)^2 + \left(\frac{\partial v}{\partial z} \right)^2 \right] + \frac{2H_z K_s N^2}{mn} - \frac{2H_z q^3}{mn B_1 l} + \frac{H_z}{mn} D_q \end{aligned} \quad (\text{C.3})$$

The boundary conditions at the top ($z = \zeta(x, y, t)$) are as follows:

$$\frac{H_z \Omega}{mn} = 0 \quad (\text{C.4})$$

$$\frac{K_q}{mnH_z} \frac{\partial q^2}{\partial s} = \frac{B_1^{\frac{2}{3}}}{\rho_0} [(\tau_s^\xi)^2 + (\tau_s^\eta)] \quad (\text{C.5})$$

$$H_z K_m \left(\frac{\partial u}{\partial z}, \frac{\partial v}{\partial z} \right) = \frac{1}{\rho_0} (\tau_s^\xi, \tau_s^\eta) \quad (\text{C.6})$$

$$H_z K_s N^2 = \frac{Q}{\rho_0 c_P} \quad (\text{C.7})$$

The boundary conditions at the bottom ($z = -h(x, y)$) are as follows:

$$\frac{H_z \Omega}{mn} = 0 \quad (\text{C.8})$$

$$\frac{K_q}{mnH_z} \frac{\partial q^2}{\partial s} = \frac{B_1^{\frac{2}{3}}}{\rho_0} [(\tau_b^\xi)^2 + (\tau_b^\eta)] \quad (\text{C.9})$$

$$H_z K_m \left(\frac{\partial u}{\partial z}, \frac{\partial v}{\partial z} \right) = \frac{1}{\rho_0} (\tau_b^\xi, \tau_b^\eta) \quad (\text{C.10})$$

$$H_z K_s N^2 = 0 \quad (\text{C.11})$$

The equation for the kinetic energy times a length scale is given as:

$$\frac{D}{Dt}(lq^2) - \frac{\partial}{\partial z} \left[K_l \frac{\partial(q^2 l)}{\partial z} \right] = lE_1(P_S + P_B) - \frac{q^3}{B_1} \tilde{W} \quad (\text{C.12})$$

Where E_1 is a constant set to 1.8. \tilde{W} is the wall proximity function, which is defined as:

$$\tilde{W} = 1 + E_2 \left(\frac{l}{kL} \right)^2 \quad (\text{C.13})$$

and

$$L^{-1} = \frac{1}{\zeta - z} + \frac{1}{H + z} \quad (\text{C.14})$$

Here E_2 is a constant set to 1.33.

A biharmonic diffusion term can also be added to this equation, which then takes the form:

$$\begin{aligned}
\frac{\partial}{\partial t} \left(\frac{H_z q^2 l}{mn} \right) + \frac{\partial}{\partial \xi} \left(\frac{H_z u q^2 l}{n} \right) + \frac{\partial}{\partial \eta} \left(\frac{H_z v q^2 l}{m} \right) + \frac{\partial}{\partial s} \left(\frac{H_z \Omega q^2 l}{mn} \right) - \frac{\partial}{\partial s} \left(\frac{K_q}{mn H_z} \frac{\partial q^2 l}{\partial s} \right) = \\
\frac{H_z}{mn} l E_1 (P_s + P_b) - \frac{H_z q^3}{mn B_1} \tilde{W} + \frac{H_z}{mn} D_{ql}. \tag{C.15}
\end{aligned}$$

D_{ql} is the horizontal diffusion for the variable ql

Appendix D

Atmospheric forcing and initial conditions creation

D.1 Atmospheric forcing creation

The data used from the ERA5 data set was downloaded hourly for the month of July 2020, with a latitude ranging from -70 to -35 and a longitude ranging from 35 to 60. This data was then interpolated onto the grid created using MATLAB scripts that are provided open source by ROMS. The variables that must be downloaded from the dataset are:

- 2m dewpoint temperature
- 2m temperature
- Mean sea-level pressure
- 10m u-component of wind
- 10m v-component of wind
- Surface latent heat flux
- Surface net solar radiation
- Surface net thermal radiation

- Surface sensible heat flux
- Surface thermal radiation downwards
- Total cloud cover
- Evaporation
- Runoff
- Total precipitation
- Eastward turbulent surface stress
- Northward turbulent surface stress

D.2 Initial conditions creation

The data used from the Copernicus Marine Service data set was downloaded daily for the month of July 2020, with a latitude ranging from -70 to -35 and a longitude ranging from 35 to 60. This data was then interpolated onto the grid created using MATLAB scripts that are provided open source by ROMS. The variables that must be downloaded from the dataset are:

- Sea water salinity
- Sea water potential temperature
- Eastward sea water velocity
- Northward sea water velocity
- Sea surface height above geoid